VPS VIBRATIONS IN PHYSICAL SYSTEMS

DOI: 10.21008/j.0860-6897.2024.1.10
Vibrations in Physical Systems, 2024, 35(1), 2024110

Investigation of flow features and acoustic radiation of a set of rectangular cavities in a channel

Paweł ŁOJEK, Katarzyna SUDER-DĘBSKA

AGH University of Krakow, al. Mickiewicza 30, 30-059 Kraków, Poland,

Corresponding author: Paweł ŁOJEK, email: lojek@agh.edu.pl

Abstract This article focuses on a noise of aerodynamic origin, generated by the flow over single and multiple rectangular cavities. The paper presents the methodology and results of the conducted numerical simulations of the air flow in a channel with a set of rectangular cavities. The aeroacoustic wave equation was used to determine the acoustic pressure generated by the flow. Various configurations of the cavities made it possible to study the influence of their reciprocal location on the generated sound. The research showed that as the distance between the cavities decreased, the acoustic pressure levels increased. They were several decibels higher than for the single-cavity case.

Keywords: aeroacoustics, numerical simulations, channel, cavity, flow, noise, HVAC.

1. Introduction

Due to the widespread use of ventilation and air-conditioning systems, the problem of noise related to the operation of these systems is becoming increasingly important. Therefore, in the case of newly developed systems, it is worth limiting potential noise sources already at the design or even construction stage of these systems. These sound sources can be of various nature - they can be both directly related to the structure itself (mechanical origin) and be the effect of air flow through the installation (aerodynamic origin).

The generation of aerodynamic noise is associated with the loss of flow stability and the appearance of turbulence [1], the causes of which can be various. In the context of air conditioning systems, the causes of turbulence in the flow include [2]:

- flow separation of a stream when flowing through the channel system,
- flow disturbance caused by a sudden change in the diameter of the channel,
- flow disturbance caused by a sudden change in flow direction,
- phenomena that may occur in the boundary layer,
- flow near protruding elements or edges.

The occurrence of these phenomena is associated with the occurrence of various discontinuities in ventilation ducts, such as branches, joints, diffusers, confusors, silencers, elbows, meshes, orifices, measuring instruments or also errors in the installation itself [3]. The object of research of this article were rectangular cavities, which can be used to model the phenomena occurring during the flow through branches, silencers, or assembly errors.

The basic geometrical parameters of cavities include length L, width W and depth D. It is not the absolute dimensions of the cavity itself that determine which type a given cavity belongs to, but their ratios. Most often, cavities are classified according to the L/D or L/W ratio, which is also related to the nature of the flow [4]. According to this classification, the cavities analyzed in this article belong to the group of shallow cavities ($L/D > 1$). The phenomena occurring in the cavities can also be classified into one of three groups: oscillations related to the dynamics of the flow, oscillations related to the interactions between the flow field and the acoustic field, and oscillations related to the interactions between the fluid and the flexible, deformable structure. In this case, the oscillations related to the dynamics of the flow and interactions between flow and acoustic fields were investigated. Above an L/W ratio equal to 1, the cavities can be treated as two-dimensional, therefore a 2D model could be investigated.

A number of studies on shallow cavities [5-12] indicate that at high-velocity flow over such cavities there is an intense acoustic radiation with the characteristic frequencies. There are self-sustained oscillations in the cavity where Kelvin-Helmholtz perturbations are amplified in the free shear layer, which interactions with the downstream corner of the cavity generate acoustic waves propagating upstream and inducing further instabilities in the shear layer [6].

According to Rockwell and Naudascher [13], flow dynamic oscillations occur when the ratio of a cavity length to a wavelength is small. They are related to the instabilities in the layer where a shear stresses occur. They are amplified by the impact of the vortices on the upstream wall in the cavity. They move along the bottom of the cavity in the direction opposite to the flow direction, after which they are carried away again by the layer in which shear stresses prevail. Some researchers [14,15] suggest that resonant acoustic mode provides the upstream feedback, which strongly reinforces the shear layer oscillation.

In this article, the object of research were shallow cavities, but in the configuration of three identical cavities. This is a solution inspired by the work of Sadamoto et all. [16], however, in the cited article, the authors focused on sound attenuation in a circular duct with a slit-like short expansion chamber, which performs as a resonant muffler in a duct, without analyzing the flow through the duct.

2. Methods and algorithms

The coupling between fluid and acoustic fields – aeroacoustic coupling, was solved using the hybrid method and aeroacoustic wave equation, developed and implemented by Schoder et al. [17]. The method is based on the assumption that the fluid flow can be decomposed into three parts [18]:

$$\phi = \overline{\phi} + \phi^{ic} + \phi^{a}, \tag{1}$$

where: $\overline{\phi}$ – mean part of the variable describing the fluid flow, ϕ^{ic}–incompressible part, ϕ^{a} acoustic part. The use of this method consists of three steps:

1. numerical simulations of fluid flow using Navier-Stokes equations with suitable turbulence model using the mesh applicable for flow simulations,
2. interpolation of flow pressure from flow mesh to acoustic mesh,
3. numerical simulations of acoustic wave generation and propagation using Aeroacoustic Wave Equation (AWE).

The Navier-Stokes equations used for the flow simulations are given by continuity (2) and momentum (3) equations [19]:

$$\nabla \cdot \mathbf{v}^{ic} = 0, \tag{2}$$

$$\rho \frac{\partial \mathbf{v}^{ic}}{\partial t} + \rho \mathbf{v}^{ic} \cdot \nabla \mathbf{v}^{ic} = -\nabla p^{ic} + \nabla \cdot [\tau] + \mathbf{f}_{\Omega}, \tag{3}$$

where: $\mathbf{v}^{ic}$ – incompressible flow velocity, p^{ic} – incompressible flow pressure, ρ – density, $[\tau]$ – viscous stress tensor, $\mathbf{f}_{\Omega}$ – external forces per unit volume.

The viscous stress tensor has to be modeled using an appropriate turbulence model. The DES (Detached Eddy Simulation) model was chosen. It is a hybrid model that combines the RANS (Reynolds-Averaged Navier-Stokes) model in the boundary layer area and the LES (Large Eddy Simulation) model at a distance from the walls.

For flow modeling in boundary layer, the $k-\omega$ SST (Shear Stress Transport) model was used. It is given by two equations that describe turbulent kinetic energy k and specific turbulent dissipation rate ω [20, 21]:

$$\frac{D\rho k}{Dt} = \tau_{ij}\frac{\partial u_i}{\partial x_j} - \beta^{*}\rho\omega k + \frac{\partial}{\partial x_j}\left[(\mu + \sigma_k \mu_t)\frac{\partial k}{\partial x_j}\right], \tag{4}$$

$$\frac{D\rho\omega}{Dt} = \frac{\gamma}{\nu_t}\tau_{ij}\frac{\partial u_i}{\partial x_j} - \beta\rho\omega^2 + \frac{\partial}{\partial x_j}\left[(\mu + \sigma_\omega \mu_t)\frac{\partial \omega}{\partial x_j}\right] + 2\rho(1-F_1)\sigma_{\omega 2}\frac{1}{\omega}\frac{\partial k}{\partial x_j}\frac{\partial \omega}{\partial x_j}, \tag{5}$$

where: $\frac{D}{Dt} = \frac{\partial}{\partial t} + u_i \frac{\partial}{\partial x_i}$ – material derivative, k – turbulent kinetic energy, ω – specific turbulent dissipation rate, β^{*}, σ_k, σ_ω, γ, a_1 – model constants, and F_1, F_2 – additional functions.

The turbulent viscosity, required by viscous stress tensor in (3) is calculated as:

$$\mu_t = \frac{\rho a_1 k}{\max(a_1\omega, \Omega F_2)}, \tag{6}$$

$$F_2 = \tanh(arg_2^2), \tag{7}$$

$$arg_2 = \max\left(2\frac{\sqrt{k}}{\beta^2\omega d}, \frac{500\nu}{d^2\omega}\right). \tag{8}$$

The DES model, which is based on the $k-\omega$ SST model, changes the variable d in the equation (8) to length scale l defined as [22]:

$$l = \min\left(\frac{\sqrt{k}}{\beta^*\omega}, C_{\mathrm{DES}\Delta}\right), \tag{9}$$

$$C_{DES} = (1 - F_1)C_{\mathrm{DES}}^{k-\epsilon} + F_1 C_{\mathrm{DES}}^{k-\omega}, \tag{10}$$

where: F_1 – function of $k-\omega$ SST model [20]; $C_{\mathrm{DES}}^{k-\epsilon} = 0{,}6$; $C_{\mathrm{DES}}^{k-\omega} = 0{,}82$ – constants of the $k-\omega$ SST DES model.

Aeroacoustic wave equation used for simulations of generation and propagation of acoustic wave is defined as [23]:

$$\frac{1}{c_\infty^2}\cdot\frac{\partial^2\psi^a}{\partial t^2} - \Delta\psi^a = -\frac{1}{\rho_0 c_\infty^2}\cdot\frac{\partial p^{ic}}{\partial t}, \tag{11}$$

where: c_∞ – speed of sound, ψ^a – acoustic scalar potential defined as $p^a = \rho_0\frac{\partial\psi^a}{\partial t}$.

The interpolation of incompressible pressure from flow to acoustic mesh was performed using nearest neighbor method. Then, on the basis of the interpolated pressure, the source terms (right hand side) of equation (11) were calculated.

This equation can be derived by using the Hardin and Pope assumption given by the (1) and rearranging the compressible Navier-Stokes equations. The hybrid method used in this work was described in greater detail in [24, 25].

3. Analyzed model and simulation parameters

As mentioned in the introduction, the analyzed model was a set of rectangular cavities in the channel. Air flow over three shallow cavities was studied. The influence of changes in the d, the distance between individual cavities, on the flow and acoustic fields was analyzed. Three cases were analyzed: for d = 0.1 L, d = 0.5 L and d = 1.0 L. As a reference model, flow calculations with the same parameters were performed, but for a single cavity. The dimensions of the analyzed model have been summarized in Table 1.

Table 1. Dimensions of the model.

Variable	Length [mm]
L	200
D	100
d	10;100;200
H	300

Due to the computational model used – a hybrid model using AWE (Aeroacoustic Wave Equation), it was necessary to use two geometric models and two computational meshes. These models are shown in Figures 1 and 2, for flow and acoustic simulations, respectively.

3.1 Initial and boundary conditions

The inlet and outlet boundaries of the flow domain have been marked in Figure 1. The remaining edges were treated as walls. The flow velocity of the air in the channel at inlet was equal to 10 m/s. The walls of the channel were treated as rigid. As described earlier, the $k-\omega$ SST DES turbulence model was used for the flow calculations. It was necessary to select the initial and boundary values of the k and ω variables. They were determined on the basis of the model author's guidelines [21,22].

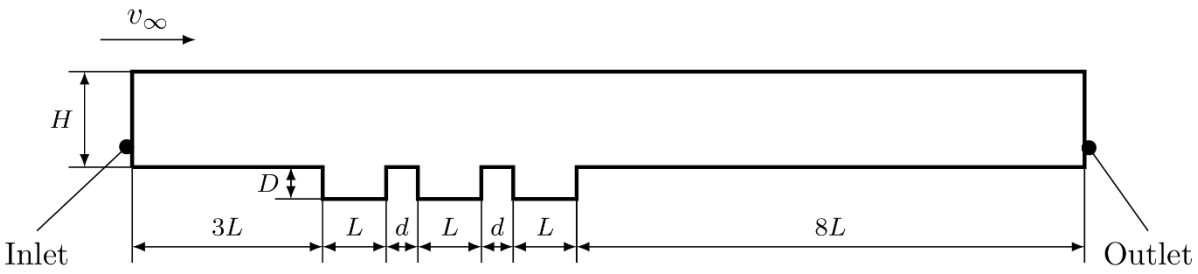

Figure 1. Geometry of the flow domain.

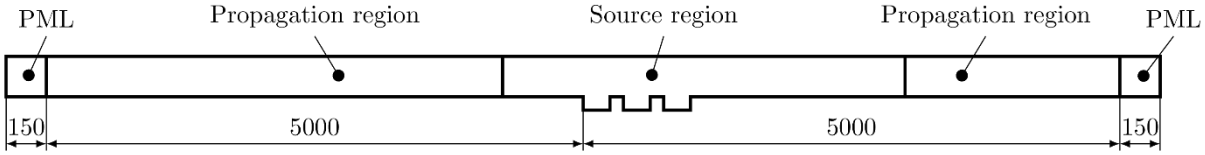

Figure 2. Geometry of the acoustic domain with marked regions.

Due to the need to ensure appropriate simulation parameters, the acoustic domain was divided into three regions, which are also marked in Figure 2. In the source region, which dimensions coincided with the flow model, the source terms were interpolated. The PML (Perfectly Matched Layer) region was introduced to eliminate reflections and ensure an anechoic end of the channel.

Simulations time was equal to 2 s. In flow simulations, a time step of $2 \cdot 10^{-5}$ s was adopted, and in acoustic simulations the time step was equal to $1 \cdot 10^{-4}$ s.

4. Results and discussion

The oscillations occurring in cavities can be described with Rossiter modes, which are defined by the equation [6]:

$$f_m = \frac{U}{L} \cdot \frac{m - \gamma}{\frac{1}{K} + \mathrm{Ma}}, \tag{12}$$

where: U – flow velocity, L – length of the cavity, m – mode number, γ – parameter used to describe the phase delay between hydrodynamic forces and the acoustic feedback, $\mathrm{M}a = \frac{U}{c}$ – Mach number and K – ratio of vortex convection speed to the flow velocity.

The parameter γ for small Mach numbers (Ma = 0.3 in analyzed case) can be taken equal to zero [26]. The parameter K, the ratio of vortex convection velocity to the flow velocity, was in this case equal to 0.65. However, the conducted tests showed that for small flow velocities this value does not always allow for the correct calculation of cavity modes [27]. It may need to be determined by research.

The first 6 Rossiter frequencies were calculated for the parameters $\gamma = 0$ and $K = 0.65$. They were equal to 31.89, 63.78, 95.67, 127.56, 159.45 and 191.34 Hz.

During the flow simulation, the following parameters were recorded: pressure loss at the flow (difference between inlet and outlet), velocity and pressure values at points placed in the center of each cavity. The results of calculated pressure losses are presented in Table 2. They show, as expected, that the introduction of additional discontinuities in the channel caused an increase in pressure drop. However, it turns out that the distances between the cavities do not significantly affect the local pressure losses.

Table 2. Calculated pressure loss.

Analyzed case	Pressure loss [Pa]	Relative difference [%]
Single cavity	5.83	–
$d = 0.1L$	7.58	29.81
$d = 0.5L$	7.64	30.91
$d = 1.0L$	7.77	33.09

Figure 3 presents the calculated spectra of flow pressure at points placed in the center of each cavity. As a reference spectrum, the spectrum for a single cavity is shown in dashed lines in each figure. For each of the analyzed distances between the cavities, the behavior of the flow in individual cavities was similar. In each case, there is a significant increase in pressure in the first cavity compared to a single cavity. There is a significant increase in pressure amplitude for $f = 12$ Hz. This may be due to some feedback caused by pressure differences resulting from turbulence and vortices occurring in successive cavities. Except that, the other components of the spectrum mostly coincide with those for the reference cavity.

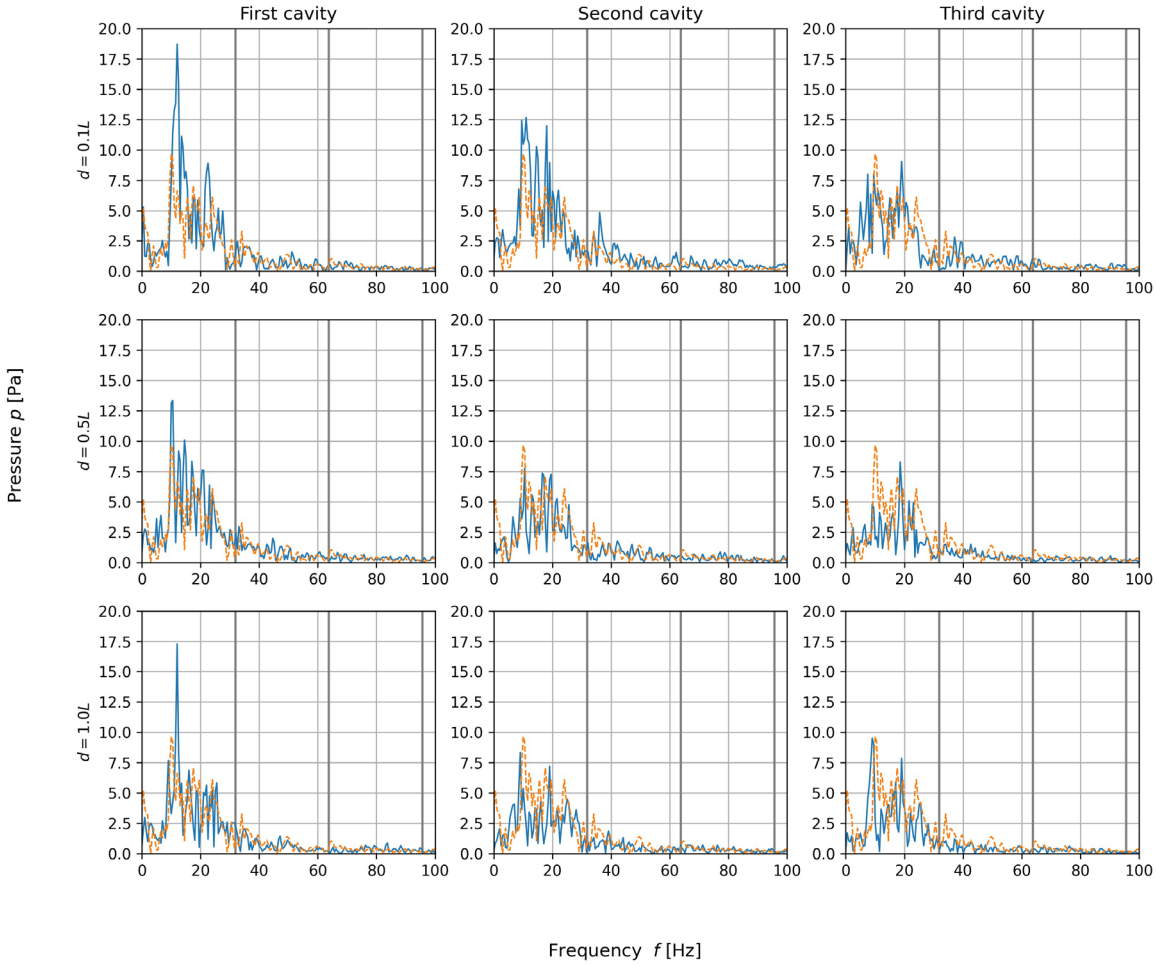

Figure 3. Spectra of pressure at the point located in the middle of each cavity (dashed lines – spectrum of pressure in the single cavity, gray lines – Rossiter modes).

The Rossiter frequencies (12) are marked in Fig. 3 with grey vertical lines. As can be seen, they do not coincide with the frequencies with the largest amplitudes. On the other hand, for the sound pressure level of the reference cavity, the first Rossiter frequency is close to the peak at 33 Hz, and the second Rossiter frequency coincides with the peak at 64 Hz. Discrepancies between the pressure signal and the Rossiter frequencies may be due to the fact that the Rossiter model was developed for flows over cavities with much higher velocities, as well as incorrect estimation of the K and γ parameters.

Next, the results of acoustic simulations will be presented. The sound pressure levels, and average sound intensity distributions were computed.

In Fig. 4, the computed sound pressure levels (SPL) for cases with set of cavities and single cavity reference case were shown. The sound pressure levels were calculated at a point located in the middle of the channel, at a distance of 4.8 m from the first cavity. Rossiter frequencies are also shown in this figure. All SPL distributions for a set of cavities are similar in nature and deviate from the spectrum for the reference case. In the case of the reference model, there is a strong agreement of some signal components with the calculated Rossiter frequencies. In the case of set of cavities, the first leading frequency is lower by

about half compared to the first Rossiter frequency, while in the case of subsequent Rossiter modes, only some are excited and only for some models.

The agreement of the results for the reference cavity with the Rossiter frequencies allows to conclude, that the results for the set of cavities are also correct. Also, it should come as no surprise that sound pressure levels are much higher in the case of three cavities than with one cavity.

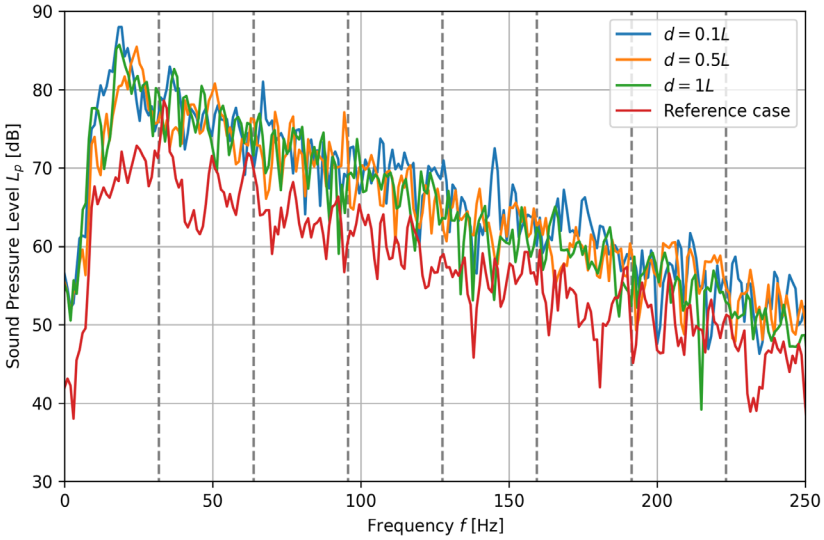

Figure 4. Sound pressure level computed for all cases at the point placed near the end, in the middle of the channel (x = 4.8, y = 0.15).

The overall sound pressure level (OASPL) in the entire band was also calculated. The results are presented in Tab. 3 and compared with the results for the reference cavity. It should be noted that the presented results are of a qualitative nature. The aeroacoustic model used may require some adjustment based on experimental data. Nevertheless, as expected, the overall sound pressure level is much higher for a set of cavities.

Table 3. Calculated pressure loss.

Analyzed case	OASPL [dB]	Difference [dB]
Single cavity	88.5	–
$d = 0.1L$	98.3	9.8
$d = 0.5L$	96.5	8.0
$d = 1.0L$	97.1	8.6

In Figures 5 – 7, the sound intensity distributions, averaged in time over 1 s, for all three cases were shown. The figures also show intensity vectors, which indicate the direction of the flow of the acoustic energy. The distributions clearly show an increase in the intensity value with decreasing distance between the cavities. The highest values were obtained for d = 0.1 L.

In each case, the main sources of noise are placed in the downstream edge of the cavity, especially the downstream edge of the third cavity. These are point sources. This behavior is also typical for single cavities [24]. However, in the case of set of cavities for d = 0.1 L, an additional linear sound source can be distinguished on the edge connecting the second and third cavities.

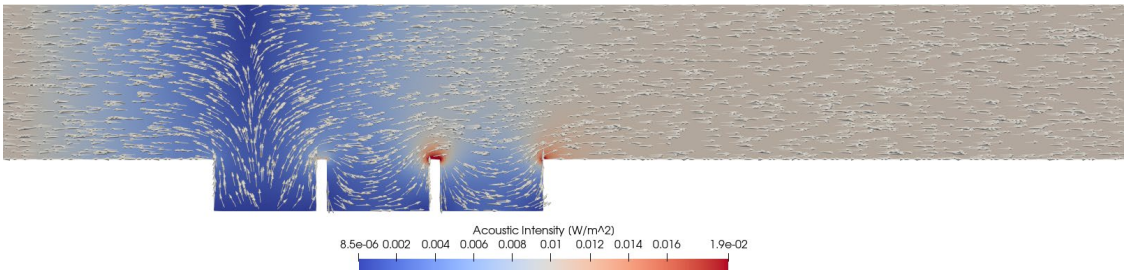

Figure 5. Average sound intensity distribution, case $d = 0.1L$.

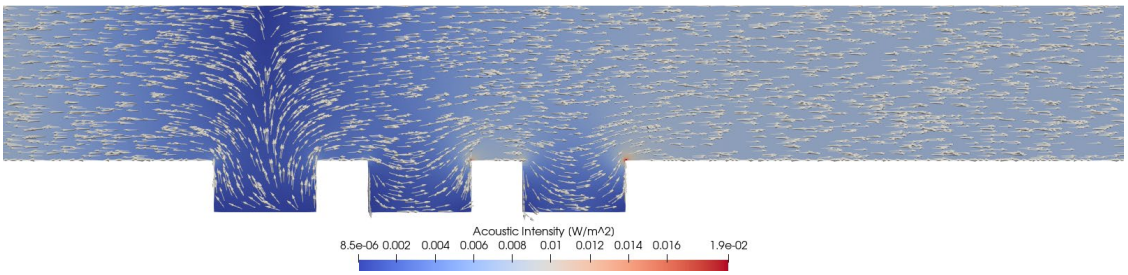

Figure 6. Average sound intensity distribution, case $d = 0.5L$.

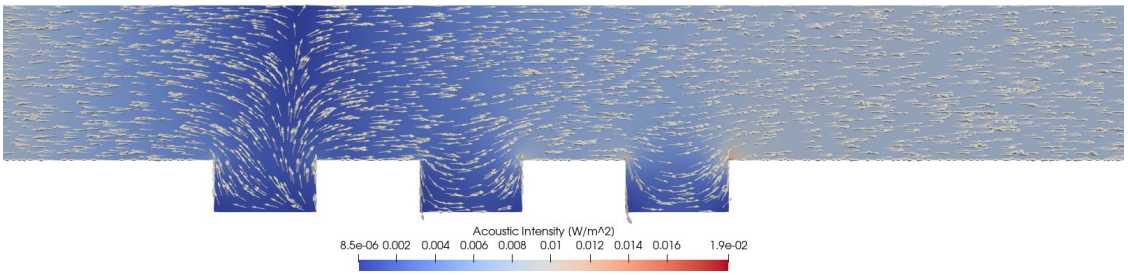

Figure 7. Average sound intensity distribution, case $d = 1.0L$.

5. Summary and conclusions

This study focuses on the influence of geometric parameters of the set of rectangular cavities on the parameters of air flow in the ventilation duct and the noise generated by the turbulent air flow. The obtained results were compared with the results obtained in the case of a duct with a single shallow cavity.

As expected, the results computed for set of cavities, regardless of the adopted configuration and distance between individual cavities differ from the results for the single cavity, an increase of pressure drop can be observed. The size of the distance between the cavities does not significantly affect the local pressure losses. Compared to the single cavity, in the first cavity for each set of rectangular cavities, the increase in the flow pressure can be observed. This increase can be related to the feedback caused by pressure gradients resulting from turbulence and vortices occurring in cavities. The highest pressure increases inside cavities were observed with spacing between individual cavities of 0.1 L. For the variant with d = 1.0 L, the pressure spectra in second and third cavity are remarkably similar to those obtained for the reference cavity. Set of cavities does not have a significant effect on other flow parameters compared to single cavity.

Regardless of the geometrical parameters (distances between cavities), a set of cavities generates higher sound pressure levels compared to the sound pressure level generated by a single cavity. The first frequency peak for a set of cavities occurs for a frequency equal to half the frequency of the first peak for a single cavity. The simulations also showed that the set of cavities for d = 0.1 L is the loudest and is louder than a single cavity by 9.8 dB.

For all analyzed variants, the downstream edge of the last cavity is the place of point source formation. For configuration number 1 (d = 0.1 L), a distinct region of sound generation can also be observed, located on the plane between the 2nd and 3rd cavity. This phenomenon is not observed for the analyzed wider distances between cavities.

In summary, as could be expected, the set of cavities can increase the pressure of the air flow in the ventilation duct and can increase the noise level generated due to this flow. However, the performed numerical studies showed that the distance between individual cavities is an important parameter affecting both the flow and the generated noise. The smaller this distance is in relation to the width of individual cavities, the higher the pressure in the flow and the higher the noise generated by this flow.

Acknowledgments

This work has been supported by national subvention no. 16.16.130.942.
We gratefully acknowledge Polish high-performance computing infrastructure PLGrid (HPC Centers: ACK Cyfronet AGH) for providing computer facilities and support within computational grant no. PLG/2023/016356.

Additional information

The author(s) declare: no competing financial interests and that all material taken from other sources (including their own published works) is clearly cited and that appropriate permits are obtained.

References

1. S. Glegg, W. Devenport; Aeroacoustics of Low Mach Number Flows; Academic Press, 2017
2. A. Fry; Noise Control in Building Services; Pergamon Press, 1988
3. E. Palmer (Ed.); Noise and Vibration Control for Building Services Systems CIBSE Guide B5; The Chartered Institution of Building Services Engineers; 2016
4. X. Gloerfelt; Cavity Noise; VKI Lectures; 2007
5. K. Karamcheti; Acoustic radiation from two-dimensional rectangular cut-outs in aerodynamic surfaces; NACA Tech. Rep.; TN 3487
6. J.E. Rossiter; Wind-Tunnel Experiments on the Flow over Rectangular Cavities at Subsonic and Transonic Speeds; Reports and Memoranda, 1966
7. H.H. Heller, D.G. Holms, E.E. Covert; Flow-induced pressure oscillations in shallow cavities; J. Sound Vib., 1971, 18(4), 545-553; DOI: 10.1016/0022-460X(71)90105-2
8. A.J. Bilanin, E.E. Covert; Estimation of possible excitation frequencies for shallow rectangular cavities; AIAA J., 1973, 11(3), 347-351; DOI: 10.2514/3.6747
9. M.B. Tracy; Cavity Unsteady-Pressure Measurements at Subsonic and Transonic Speeds; vol. 3669; NASA, Langley Research Center, 1997
10. G. Ashcroft, X. Zhang; Vortical structures over rectangular cavities at low speed; Phys. Fluids, 2005, 17(1), 015104; DOI: 10.1063/1.1833412
11. V. Thangamani, K. Knowles, A.J. Saddington; The effects of scaling high subsonic cavity flow oscillations and control; J. Aircraft, 2014, 51(2), 424-433; DOI: 10.2514/1.C032032
12. J.L. Wagner, S.J. Beresh, K.M. Casper, E.P. DeMauro, S. Arunajatesan; Resonance dynamics in compressible cavity flows using time-resolved velocity and surface pressure fields; J. Fluid. Mech., 2017, 830, 494-527; DOI: 10.1017/jfm.2017.606
13. D. Rockwell, E. Naudascher; Review – Self-sustaining oscillations of flow past cavities; J. Fluid. Eng.; 1978, 100(2), 152-165; DOI:10.115/1.3448624
14. C.K. Tam, P.J.W. Block; On the tones and pressure oscillations induced by flow over rectangular cavities; J. Fluid Mech., 1978, 89(2), 373-399; DOI: 10.1017/S0022112078002657
15. S. Ziada, P. Lafon; Flow-excited acoustic resonance excitation mechanism, design guidelines, and counter measures; ASME Appl. Mech. Rev, 2014, 66(1), 010802; DOI: 10.1115/1.4025788
16. A. Sadamoto, Y. Tsubakishita, Y. Murakami; Sound attenuation in circular duct using slit-like short expansion of eccentric and/or serialized configuration; J. Sound Vib., 2004, 277, 987-1003; DOI:10.1016/j.jsv.2003.09.028
17. S. Schoder, C. Junger, M. Kaltenbacher; Computational aeroacoustics of the EAA benchmark case of an axial fan; Acta Acust., 2020, 4(5), 22; DOI:10.1051/aacus/2020021

18. J.C. Hardin, D.S. Pope; An acoustic/viscous splitting technique for computational aeroacoustics; Theor. Comp. Fluid Dyn., 1994, 6, 323-340; DOI:10.1007/BF00311844
19. J. Blazek; Computational Fluid Dynamics. Principles and Applications; Elsevier Ltd. 2015
20. F. Menter; Zonal two equation k- ω turbulence models for aerodynamic flows; 23rd Fluid Dynamics, Plasmadynamics, and Lasers Conference, 1993
21. F. Menter; Two-equation eddy-viscosity turbulence models for engineering applications; AIAA Journal, 1994, 32(8), 1598-1605; DOI:10.2514/3.12149
22. M. Strelets; Detached eddy simulation of massively separated flows; 39th Aerospace Sciences Meeting and Exhibit, 2001
23. M. Kaltenbacher; Theoretical Acoustics. Part: Aeroacoustics; Graz University of Technology, 2021
24. P. Łojek, I. Czajka; Impact of cavity edges shape on aerodynamic noise; Vib. Phys. Sys., 2022, 33(3), 2022301; DOI:10.21008/j.0860-6897.2022.3.01
25. S. Schoder *et all.*; Application limits of conservative source interpolation methods using a low Mach number hybrid aeroacoustic workflow; J. Theo. Comp. Acous., 2021, 29(1), 1-27; DOI:10.1142/S2591728520500322
26. R. Ma, P. Slaboch, S. Morris; Fluid mechanics of the flow-excited Helmholtz resonator; J. Fluid Mech., 2009, 623, 1-23; DOI: 10.1017/S0022112008003911
27. P. Łojek, I. Czajka, A. Gołaś; Numerical Study of the Impact of Fluid-Structure Interaction on Flow Noise over a Rectangular Cavity; Energies, 2022, 15(21), 8017; DOI:10.3390/en15218017